
Article:
Shaw, David orcid.org/0000-0001-5542-0334 and Wagenaars, Erik orcid.org/0000-0002-5493-3434 (2019) Modelling radio-frequency plasma cleaning of fusion optics. Plasma Physics and Controlled Fusion. 085031. ISSN 1361-6587

https://doi.org/10.1088/1361-6587/ab2cb2

Modelling radio-frequency plasma cleaning of fusion optics

OPEN ACCESS
IOP Publishing
Plasma Physics and Controlled Fusion
Plasma Phys. Control. Fusion **61** (2019) 085031 (12pp)
https://doi.org/10.1088/1361-6587/ab2cb2

Modelling radio-frequency plasma cleaning of fusion optics

David Shaw[1] **and Erik Wagenaars**

York Plasma Institute, Department of Physics, University of York, York, YO10 5DD, United Kingdom

E-mail: david.shaw@york.ac.uk and erik.wagenaars@york.ac.uk

Received 18 February 2019, revised 5 June 2019
Accepted for publication 25 June 2019
Published 11 July 2019

Abstract

Metallic mirrors are to be used extensively within ITER for diagnostics and real time control. Erosion of the first wall within ITER will cause particles to be redeposited around the machine, including on these first mirrors, which will cause a reduction in reflectivity and a degradation in quality of signal received by the detectors. Powering these mirrors to form capacitively-coupled plasmas (CCPs) with an induced self bias, and using the ions within the plasmas to bombard and remove the deposits, has shown some experimental success in recovering mirror reflectivity. In this work the ion energy distribution functions (IEDFs) from an Ar CCP formed on a 5 cm radius metallic mirror are modelled and investigated using the hybrid plasma equipment model. Initially a geometry variation is done showing that a simple increase in reactor volume can significantly impact the spatial distribution of the ion flux to the mirror surface leading to non-uniform etch rates across the surface, even after the maximum bias has been achieved. The ion energies need to be sufficient to remove depositions (focussing on the first wall material of Be which forms a surface oxide BeO) but not subsequently damage the underlying mirror. In order to achieve this both the voltage (50–1000 V) and the frequency (13.56–60 MHz) have been varied within the model showing trends that may lead towards IEDF optimisation. The increase in voltage increases the self bias linearly and the plasma density super-linearly, whereas increasing the frequency barely effects the self bias while increasing the plasma density sub-linearly. Both increases cause an increase in ion flux for these reasons but both also decrease the homogeneity of the ion flux across the mirror surface which will be required should the energies be above the threshold for the mirror. These results are also unique to the geometry being investigated and thus the conclusion is that it would be prudent to model individual mirror geometries to find optimal parameters. This becomes especially clear with the introduction of a perpendicular magnetic field into the simulation that significantly reduces electron transport within the plasma.

Keywords: hybrid simulation, fusion optics, ion energy distribution function, etching, beryllium oxide

(Some figures may appear in colour only in the online journal)

1. Introduction

The design of the ITER includes multiple optical diagnostic systems. These diagnostics rely on metallic mirrors in close proximity to the fusion plasma to gather optical information, and direct it down shielded pathways. With the high flux of particles from the fusion plasma impacting the Be first wall, and W divertor, the surfaces will be eroded. Erosion of mirrors themselves is not considered an issue as the surface can be maintained using materials with an ordered structure or

[1] Author to whom any correspondence should be addressed

small-scale crystals [1]. However the material eroded from the first wall will deposit on these optics and cause reduced reflectivity which degrades the quality of the signal received by the diagnostic detectors [2–4].

This issue is one that has found a proposed solution [5]. The mirrors, being stainless-steel, molybdenum, or rhodium-coated molybdenum, are all metallic and therefore can be used as a powered electrode to form a capacitively-coupled plasma (CCP) [6, 7]. The ions created within this plasma can then be attracted to the surface with sufficient energy to sputter the deposited material using a self-bias voltage [8]. This is physical etching and is a well understood process that is used extensively in the manufacturing of microprocessors [9, 10]. It is known that when forming a CCP a difference in ratio between grounded and powered electrode areas causes the formation of a self bias. This is from circuit theory where a smaller powered electrode will have a smaller capacitance which increases the sheath width up to that of the RF amplitude [11]. This is then compounded through the use of a blocking capacitor between the electrode and the AC supply which stops the electrons, that have reached the surface during the RF cycle, from flowing to ground [12]. This imparts a DC component which further increases the sheath width such that ions may accelerate to an energy that is a combination of the plasma potential and the self bias voltage.

This method has been successfully tested within the laboratory environment multiple times [5, 7, 8, 13–16]. However, exact optimisation of the procedure is very challenging in experiments since the important self bias effect critically depends on the system's geometry. In particular the distances between the powered electrode and any grounded components nearby. The effects of the geometry will need to be understood first before further optimisation can be addressed e.g. voltage and frequency variations. With vacuum chambers being expensive pieces of equipment the size of a reactor is usually just sufficient for the experiment they are designed for and no larger. Some work has been done looking at very close grounds [17], but these were wire mesh and cannot represent permanent internal mirror housing geometries. In most CCP reactors, designed primarily to investigate semi-conductor etching, there is a parallel grounded electrode. Within ITER the only ground for a powered mirror will be the nearest wall. The orientation and distance of this wall from the electrode will change the distribution and energies of ions impacting the surface of the mirror which will change the etching profile. Replication of ITER-relevant geometries is clearly challenging experimentally, therefore, modelling studies are more appropriate at this stage.

In this paper the impact of geometry on ion energy distribution functions (IEDFs) is shown. Also investigated are IEDF changes in one geometry with variations in voltage and frequency. The gas used throughout this work is Ar as it has been used extensively in the published work and has also been suggested as the working gas for this on ITER [7, 8, 13–17]. Also in this paper are some brief results on the impact of a small perpendicular magnetic field which are shown and discussed.

When considering the energies of the ions it is important to know what a useful etching energy is. Most of the deposits within ITER will be BeO for which no experimental sputtering data using Ar ions could be found. Although the, previously cited, experiments have been done they have not provided energy thresholds. Any data available is mainly theoretical and is focussed on light ions, where the Bodhansky formula for sputtering yield may be used [18]. Comparisons from work done by Moser give BeO about half the sputtering yield as Al_2O_3 in Ar at a 200V bias [7]. However these are based on fits from Yamamura which have limited data at the lower energy levels [19]. It is also contrary to etching with D_2 which is a lower mass ion but for which BeO has a lower threshold energy than Al_2O_3 by more than 50% (29–66 eV respectively) [16]. It has also been shown by Moser that BeO etches faster when bombarded with Ar ions as opposed to lighter elements, such as He or H_2 [14], but no direct experimental comparison for sputtering thresholds has been found. With the limited data available an informed estimation of a sputtering threshold of 25 eV has been made for BeO under bombardment from Ar ions. This is half of that of Al_2O_3 [20, 21].

2. Methods

For this work the hybrid plasma equipment model (HPEM) was used. This is a 2D modular plasma simulation code for simulating low-temperature plasma sources. This code was developed by Mark Kushner and collaborators with a simple description given here and a more comprehensive detailing of the code found in [22–25].

The modules used throughout are the electro-magnetics module (EMM), which takes inputs of currents, properties of boundary materials, and plasma conductivity to solve Maxwell's equations. The EMM outputs vector components and phase of electric and magnetic fields which are fed into the electron energy transport module (EETM). This in turn outputs electron sources and impact rate coefficients, derived from the solution to the Boltzmann equation, which are passed into the fluid kinetics Poisson module (FKPM). The FKPM solves for ion and neutral transport, with associated fields, using Poisson's equation.

As this work is done at low pressures $<$75 mTorr, where non-local electron heating is significant in CCP sources [26, 27], the electron transport cannot be dealt with sufficiently using a fluid momentum equation. The electron Monte-Carlo Simulation (eMCS) is used where pseudo particles are released from random numeric cells and their paths integrated in the electric fields produced by the FKPM. The initial location of the pseudo particles is according to the electron density, also generated within the FKPM. Collision rates for electrons are determined using collision cross-sections from a gas phase chemistry input file. The time step used for advancing the particle is stochastic, as is such with a Monte Carlo method, and the details can be found in [28]. The pseudo particle is then integrated through that time step and collisions are stochastically determined to have occurred

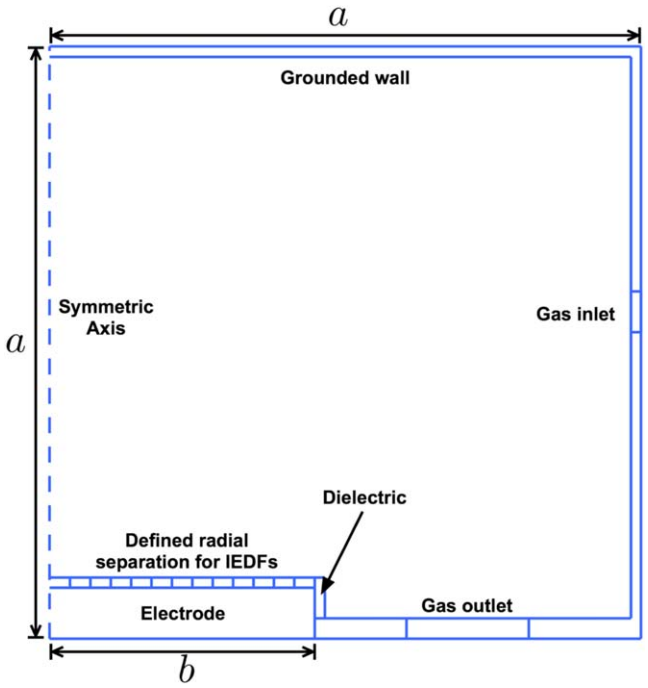

Figure 1. Geometry used in this work. The height and radius of the geometry, a, varies between 11.8 and 47.2 cm. The electrode radius, b, is between 5 and 5.6 cm.

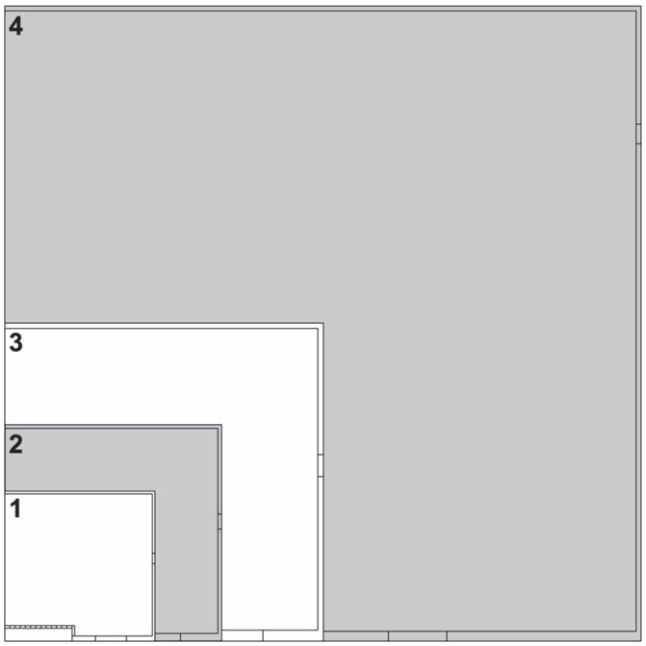

Figure 2. Visual representation of variation in geometries. The height and radius of the various geometries are, in order from 1 to 4; 11.8, 17.7, 23.6, and 47.2 cm.

or not. If the collision occurs then the collision type and scattering angle are also randomly assigned. Else if no collision occurs then the particle is integrated through another time step. Over a number of RF cycles statistics are gathered and an electron energy distribution is output for each location. The electron impact rate and transport coefficients are then calculated and fed back into the FKPM. The FKPM and EETM iterate through these above processes multiple times in order to reach convergence.

Fluid equations are used to solve for the heavy species transport, which means that energies and angular distributions are not available for the calculation of the IEDFs at the electrode surface. To access IEDFs the Monte Carlo techniques, similar to the ones used in the eMCS, are utilised in the particle-in-cell Monte Carlo module in the final iteration of the code. The gas phase collisional processes use the same reaction mechanism as in the FKPM. The particle trajectories are followed until they strike a surface at which point energies and angular distributions are output [29]. The gas phase chemistry used in this work is argon and has been validated and used in other works such as [30–32]. The species in the simulation are Ar, Ar^+, $Ar(1s_1)$, $Ar(1s_2)$, $Ar(1s_3)$, $Ar(1s_4)$, Ar(4p), Ar(4d), $Ar_2(^3\sum_u^+)$, Ar_2^+, and e^-. Neutral Ar gas flows in at a rate of 30 sccm and a pressure of 10 mTorr is maintained through a calculated flow out of the reactor. The working pressure of 10 mTorr is chosen as it has been suggested as a useful working pressure for this deposition removal method on ITER [17].

In order to investigate the effect of geometry on the plasma properties, in particular IEDFs, a simple geometry, shown in figure 1, is considered. The reactor height and radius, a, and the electrode radius, b, are varied. The variations in reactor volume are shown in figure 2. In each case the electrode radius remains roughly the same size between 5 and 5.6 cm while the volume of the reactor increases. The reason that the electrode radius is not exactly constant is the limitation imposed by the geometry mesh which changes with the change in overall reactor size. The mesh must be small enough to resolve the plasma accurately, but not so small that the computational time becomes unreasonable or that the ions travel non-locally. The cell sizes therefore increase with each geometry and are 0.2 cm^2, 0.4 cm^2, 0.8 cm^2, and 1.6 cm^2 for geometries 1–4 respectively. The geometries are all cylindrical about the symmetric axis and have geometry defined spatial variation on the electrode surface for recovery of the IEDFs radially.

For the geometry variations the power was supplied to the lower electrode at 130 V and 13.56 MHz. There have been suggestions that frequencies as high as 60 MHz may be used for this cleaning method, but most published experiments have been done at 13.56 MHz. The voltage was not varied and the self bias is calculated by the code and was not set. Any changes in the plasma potential or self bias are therefore products of the geometry.

For the voltage variations 50, 200, 300, 500, and 1000 V were analysed. Each one was done within the smallest of the simple geometries (geometry 1 in figure 3) and at 13.56 MHz. The pressure was not varied and remains at 10 mTorr throughout. This was also kept constant for the frequency variation through the harmonics of 13.56 MHz (13.56, 27.7, 40, and 60 MHz).

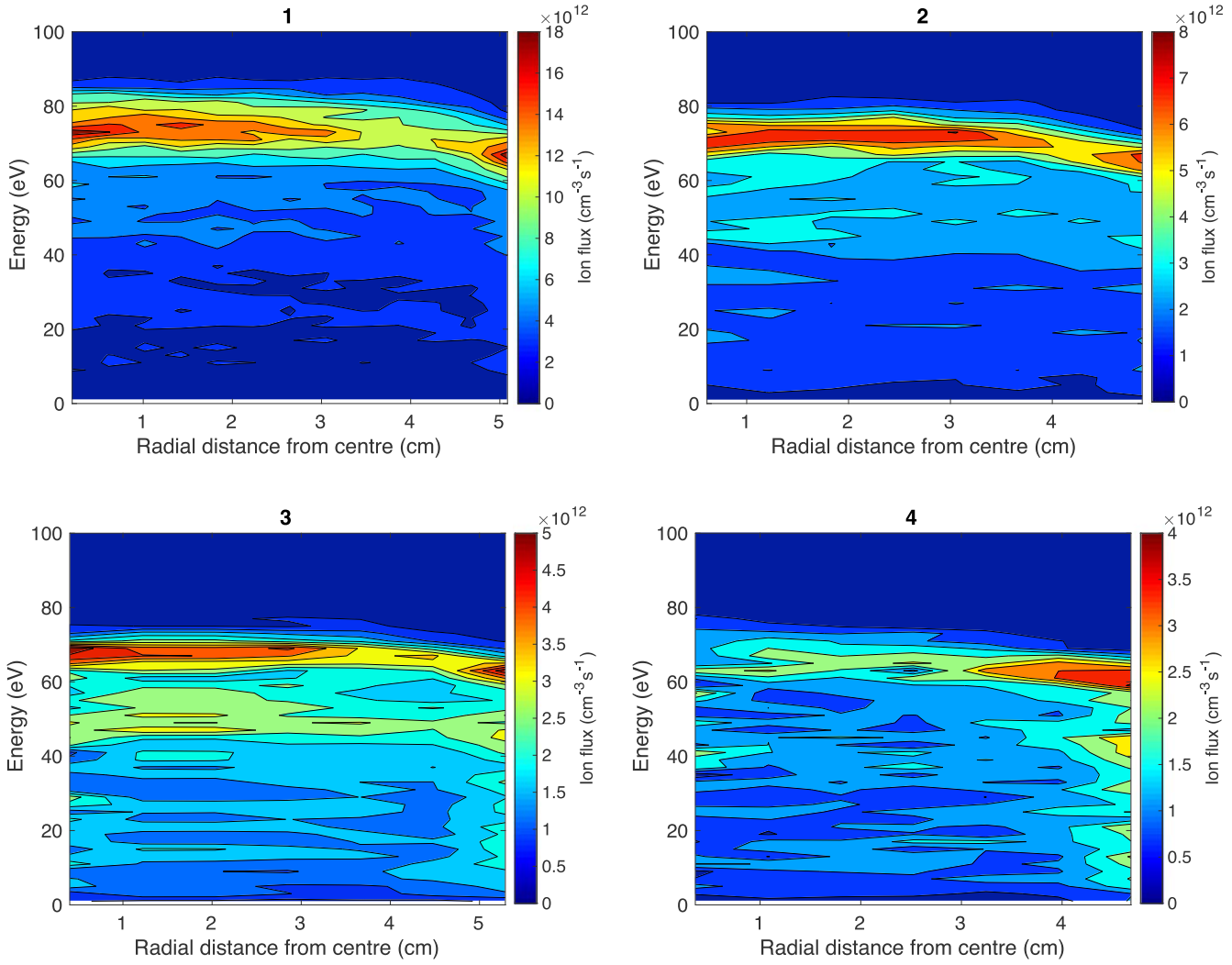

Figure 3. Total ion flux and energies for the geometry variations.

3. Results and discussion

3.1. Geometry variation

In figure 3 the variations in ion energy and flux for the different geometries are shown. The trends with the increasing reactor volume are decreases in peak flux and maximum energy. In all cases there is a peak in total flux at the edge of the electrode due to increased fields from standing waves. These are due to surface waves propagating radially into the discharge at these high frequencies [11, 33, 34]. The flux difference is shown more clearly in figure 4 where it appears less disjointed than in figure 3. Ignoring the results from geometry 4 for a moment, in both figures the minimum flux for the geometries lies at a dip between a central peak, caused by the high plasma density above the centre of the electrode, and outer peak from edge effects. This is not unusual for CCP devices. Edge effects, undesirable in manufacturing due to inhomogeneity, can be ignored by having any surface to be etched much smaller than the electrode itself. This is not the case for fusion optics as the whole electrode is the mirror. Geometry 1 is the only geometry where the maximum flux is

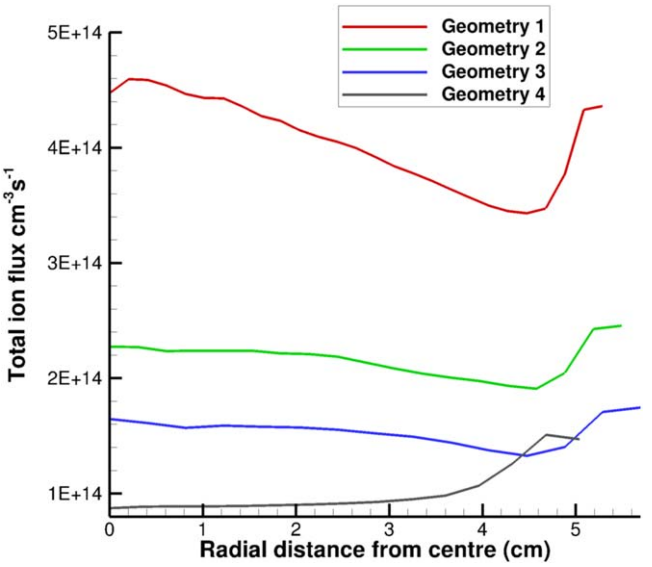

Figure 4. Total ion flux at the electrode surface for each geometry.

Table 1. Values for measured maximum plasma potential and self bias in the simple geometries.

Geometry	Plasma potential and self bias (V)
1	24.7, −58.8
2	23.0, −56.0
3	20.6, −51.8
4	8.8, −71.1

at the centre of the electrode where the bulk plasma is dense enough to provide more ions than procured by the edge effects. However, geometries 2 and 3 present a more homogeneous etch across the majority of the electrode surface which would be more desirable when attempting to maintain the mirror shape should etching continue beyond the oxide layer.

With the threshold energy taken into consideration, in the introduction to this paper, it can be seen that within these parameters the energies are much higher than those required to etch BeO (>25 eV). This is good as it means that in all cases the deposits would be removed from the surface. However the etching threshold for Mo, the material out of which a substantial number of mirrors will be made, is only 35 eV [19]. Removing the deposits may not be useful if the underlying mirror is also damaged, especially if that damage is non-uniform etching that deforms the mirror surface.

The distribution of energies shows that in geometries 1 and 2 there is a single peak of ion energies across the majority of the electrode. Geometry 3 shows a more bimodal structure with a second peak forming at about 50 eV corresponding to the minimum sheath potential. In each case, from geometries 1–3, there is an increase in lower energy ions which will pay a role in the etching process. Any ions below the sputtering threshold could be made up of previously sputtered material and thus could be a source of re-deposition. The low energy ions will neutralise on the surface of the mirror and redeposit.

From table 1 the values for the self bias and plasma potential can be seen. When considering the self bias of a system the accepted theory is that as the grounded area increases in relation to the powered area the self bias will increase. This is due to the flow of current to the ground increasing which needs to be balanced. This increase is not seen in this work. In this simple geometry the input voltage is already at the maximum required to balance the current and thus no further increase in the grounded area will change the bias voltage. However when we reach geometry 4 an extreme case is seen where the plasma potential drops and the self bias increases dramatically. The effects of this can be seen in figures 3 and 4. The drop in plasma potential and increase in the self bias can be explained by the orientation and surface area of the available ground. Either the initial plasma that is invoked at the start of the simulation is unsustainable, and should the simulation be run for an increased time period then quenching may occur, or the plasma is sustainable but potentially only as a coronal discharge around the electrode. The electric fields of geometries 3 and 4 are compared in figure 5 where the electric field is not seen for the vast majority of geometry 4. A lack of connection with the ground suggests that the plasma is in fact quenching and would not be sustainable for removing deposits. This may be checked with an increased run time, however, with this simulation already taking over a month to run, the result not impacting this work substantially, and HPEM failing to output on a quenched plasma, the simulation time was not increased. The simulations themselves were mainly run on four threads on Intel Xeon E5-2683 v4 2.1 GHz processors housed within a Dell PowerEdge R630. Only some of HPEMs modules are parallelised and we found that running on four threads provided a factor of three decrease in run time which did not decrease much further with increased thread count.

3.2. Voltage variation

As ITER is now in the building stage and designs for the machine are set it is clear that geometry is not a feasible optimisation parameter but instead a set boundary condition. One variable that may be adjusted in order to optimise IEDFs in fixed mirror geometries is the voltage.

Figure 6 shows the ion flux and energies for the varying voltages and also shows a linear relationship with the self bias and the input voltage. As expected the maximum ion energies are at the sum of the bias voltage and the plasma potential in each case with the bottom of the main band of ions sitting at the bias voltage. Any ions with energies below the bias voltage must be ions that have undergone collisions in the sheath, they have either simply lost energy, or they have transferred charge to a neutral through charge exchange. For each increase in voltage the energy of the ions shifts upwards as expected while maintaining a similar structure. The band of high energy ions across the surface of the electrode widens as the voltage increases, but this is an expected result considering the divergence of the plasma potential and the self bias. The number of low energy ions also decreases comparatively to the overall flux implying reduced redeposition with increased voltage.

The total flux can be seen in figure 7(a) which also shows a more homogeneous flux at the lower voltages. This does not come across as easily in figure 6 where the overall flux shape may appear to be fairly similar in each case. The large spread of energies masks the flux inhomogeneity across the electrode surface in the contour plots. Figure 7(b) also shows that the average increase in flux is super linear with voltage, by comparing the maximum and minimum flux for each voltage the inhomogeneity is also shown to follow this trend. Increasing the voltage would therefore decrease etching time dramatically, reducing the re-deposition rate along with increased etching. However the non-uniformity of the etch would increase at the same rate and given the energies the damage to the underlying mirror would be unavoidable, especially at the edge. Therefore there is a trade off between etch uniformity and rate, but with a requirement to maintain mirror performance after deposition removal the decision should be made to reduce the rate and protect the mirror. Therefore the recommendation regarding implementation of this method, for this specific geometry, would be to keep the

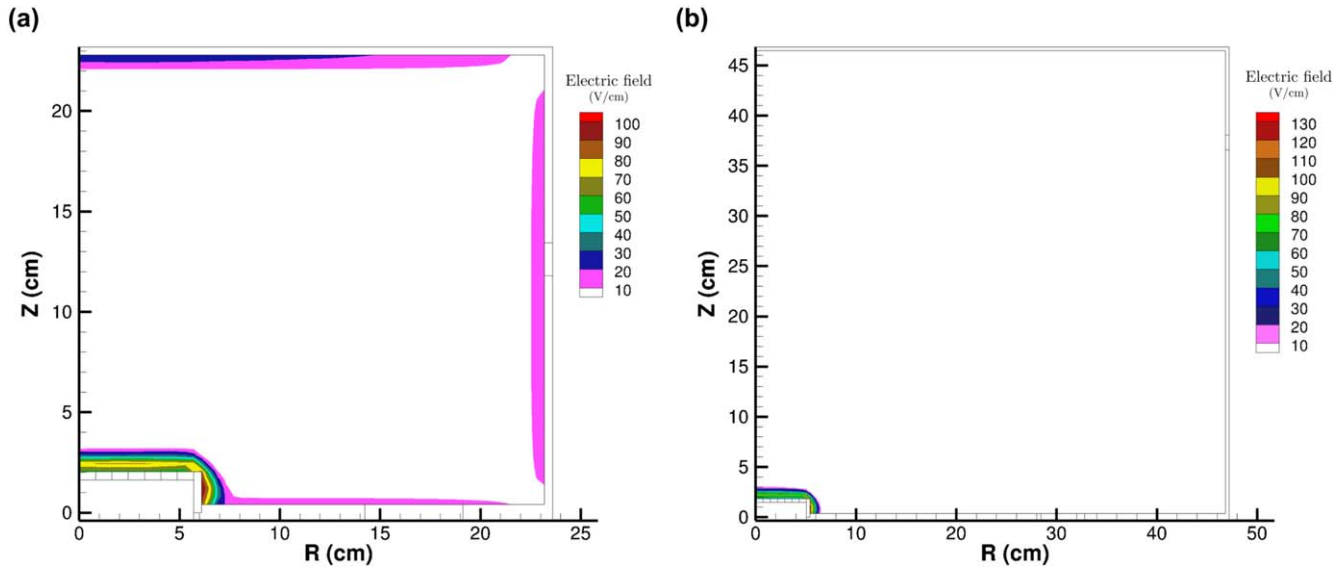

Figure 5. The electric field for geometries 3 (a), and 4 (b).

voltage low enough to maintain ion energies below the 35 eV etching threshold of the mirror.

3.3. Frequency variation

It is known that increasing the driving voltage frequency of a discharge will increase the plasma density, and ion current, while maintaining the maximum ion energy (assuming the geometry, pressure, and voltage remain constant) [35]. Simulations were run at various harmonics of 13.56 MHz in geometry 1 at 130 V; the ion energy and flux as a function of electrode radius are shown in figure 8. With the increasing frequency the width of the ion energy distribution reduces with the sheath width. This is useful for etching as the finer band of energetic ions can lead to better tuning of the system, especially to fit the main band of ions between the threshold energy of the deposits at 25 eV and that of the mirror at 35 eV. The number of low energy ions also decreases with the sheath width due to the reduced distance within which collisions can occur.

Figure 9(a) shows the increase in frequency causes the flux to grow more at the centre of the electrode than at the edge which is due to an overall increase in plasma density shown in figure 11(a). This can be viewed as a multiplication that increases the areas of high density more than it increases in the areas where it is low. The greater number of ions in the high density areas gives rise to higher flux. This will give a less uniform etch with higher frequencies, which is not ideal when the threshold energies of the deposits and the mirrors are so close. The range of energies is thinnest at 60 MHz and is between ∼58 and ∼65 eV. Reducing the voltage could bring the maximum energy below the 35 eV threshold while maintaining the majority of the flux above the assumed 25 eV BeO etching threshold. This removes the necessity to have a uniform etch as damage to the mirror is not possible below the threshold energy. When attempting this the lowest voltage at which a 60 MHz plasma would sustain within this geometry was 75 V. At these parameters the ion energies were seen to be between ∼38 and ∼47 eV over the majority of the electrode which would still etch the underlying mirror and require homogeneity. Lowering the frequency to 40 MHz allowed the plasma to exist with 50 V and give a band of ions within the assumed optimum range. This result is shown in figure 10. It should be stressed that these optimal parameters depend strongly on the geometry and will differ between experimental geometries.

The flux increase with frequency is different from that seen with voltage, as shown in figures 7(b) and 9(b). The increase is very slightly sub-linear with frequency but super-linear with voltage, which is expected. Figure 11 shows that as both the voltage and frequency increase, the plasma density increases and, that being so, there are more ions in the plasma in general. With the increase in frequency the bias voltage decreases only by a few volts but with voltage the bias increases significantly.

3.4. Influence of a magnetic field

Something that has been left out of the work so far, but something that will be a principal challenge on ITER, is the influence of a magnetic field on the removal process. It has not been included in the previous work for simplicity, and also as the majority of the experimental work done in this area has also been without a magnetic field present. As a small indication of the potential issues that may be faced, a simulation was run in geometry 1, at 13.56 MHz, 130 V, 10 mTorr, and with a 100 G vertical magnetic field. Details on how external magnetic fields are implemented in HPEM can be found in [22, 36]. The magnetic field strength is two orders of magnitude lower than would be found in ITER, however, as the cyclotron motion requires small time steps the strength was kept low to keep simulation times pragmatic. This small magnitude homogeneous field still shows significant induced changes.

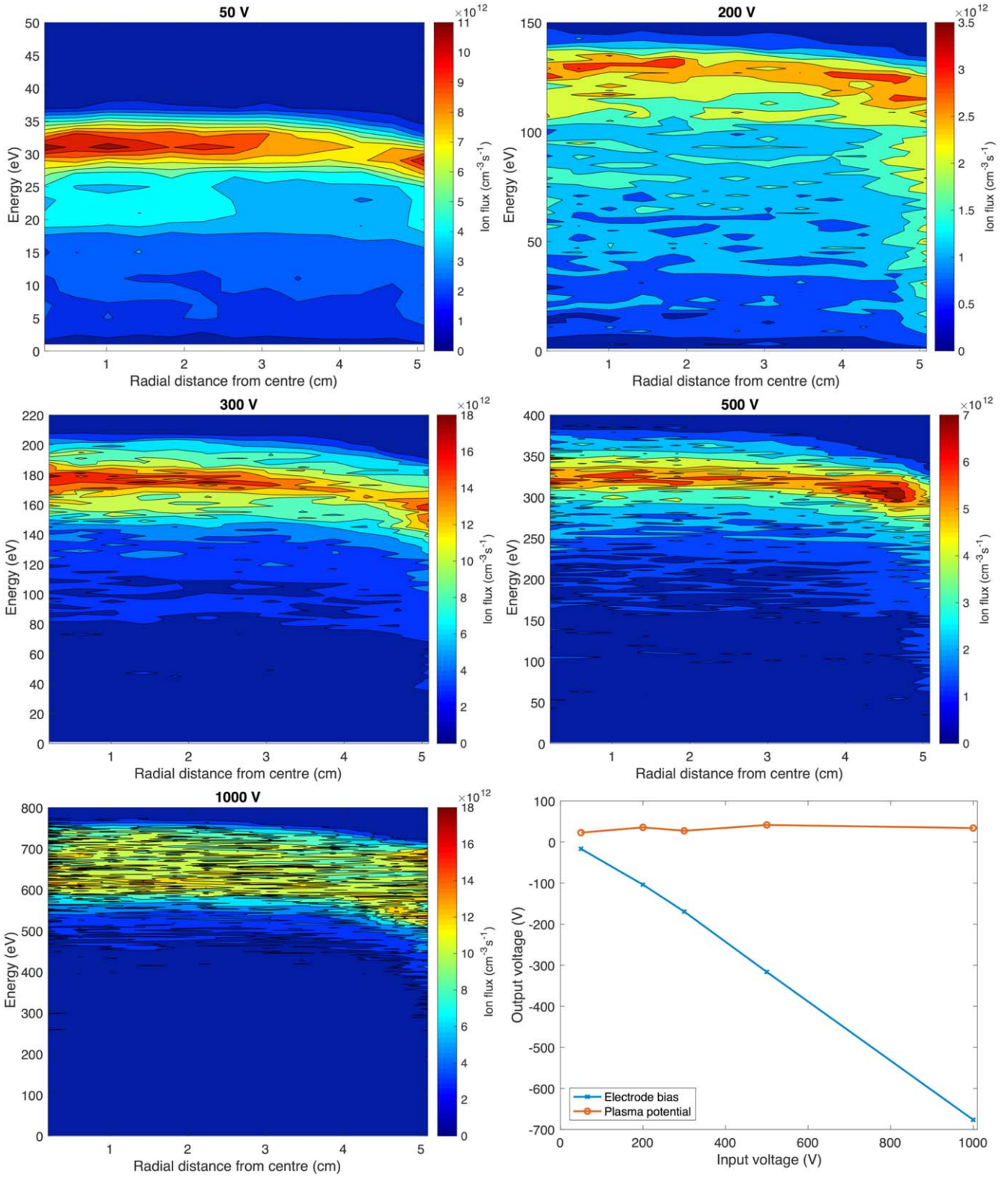

Figure 6. Ion energies and total flux as a function of radius for varying voltages at 10 mTorr in geometry 1. The plasma potential and electrode bias as a function of input voltage is also shown.

Figure 12 (a) shows the reduction in energy of ∼20 eV for the ions across the electrode but the spread of energies remains almost the same as without the magnetic field in figure 12 (c). The ion flux is completely different with the magnetic field, as shown in figure 12 (b). Overall it is reduced to less than half of its non-magnetic field value with the lowest flux value of the magnetic case of 1.5×10^{14} cm^{-3} s^{-1} corresponding to a non-magnetic value of 4.5×10^{14} cm^{-3} s^{-1}, and the peak in the magnetic case of 2.1×10^{14} cm^{-3} s^{-1} corresponding to 4.3×10^{14} cm^{-3} s^{-1} for the non-

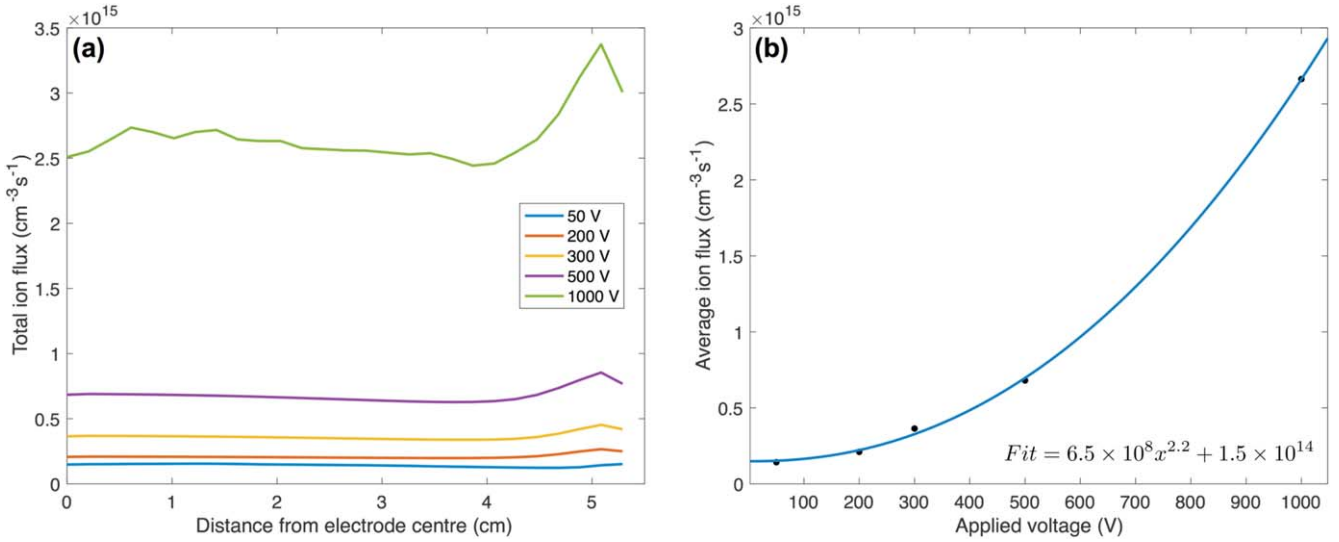

Figure 7. Total ion flux variations on the powered electrode as a function of input voltage. (a) Shows the spatial distribution of the flux with electrode radius and (b) gives the average flux as a function of input voltage.

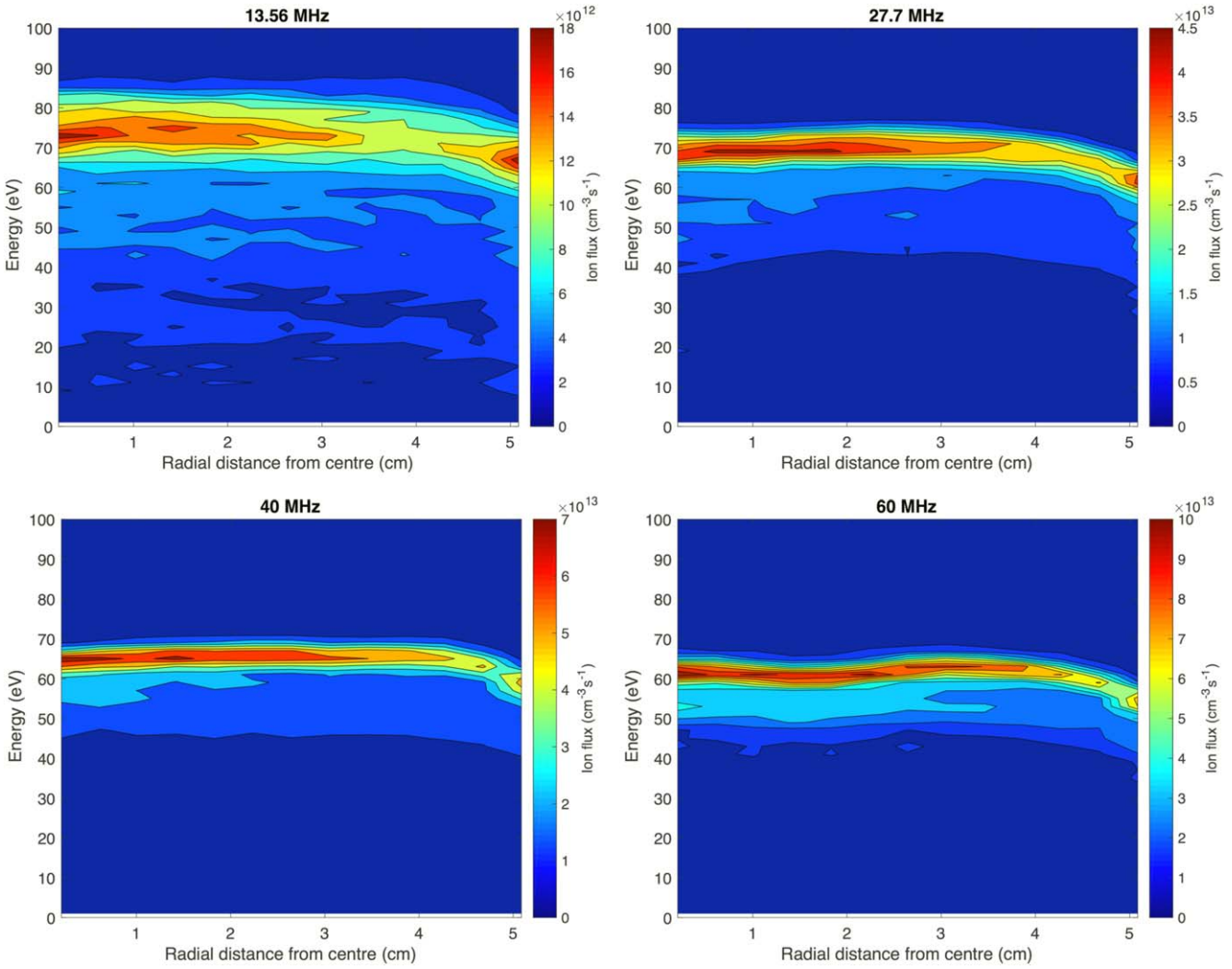

Figure 8. Geometry 1 total ion flux and energy as a function of electrode radius for various harmonics of 13.56 MHz.

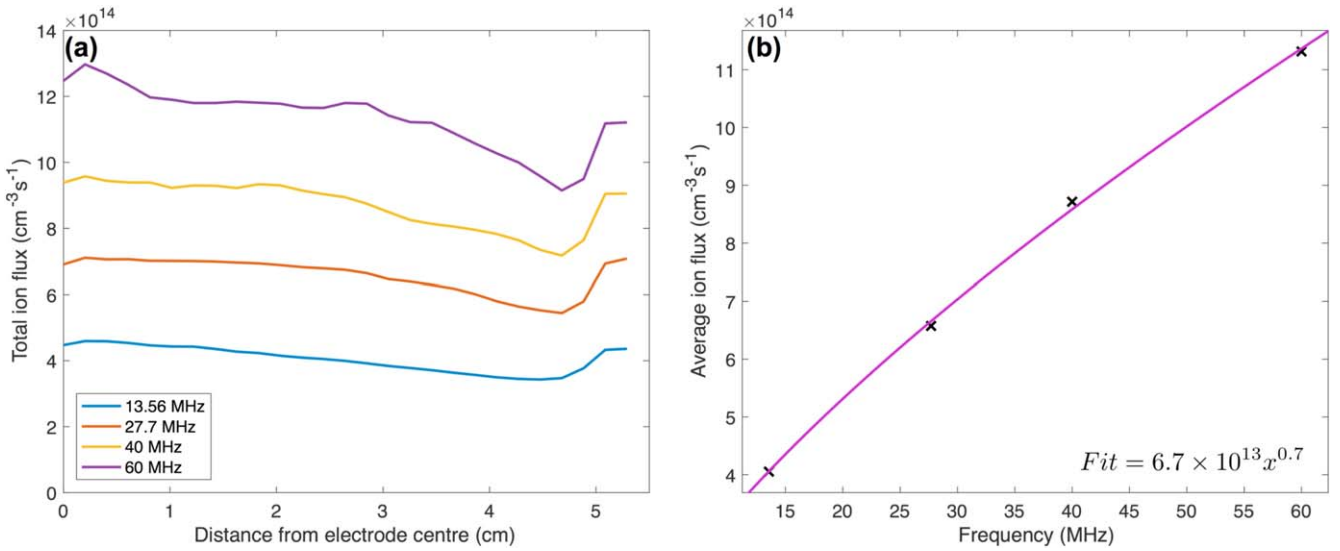

Figure 9. (a) Total ion flux versus electrode radius with varying frequencies, and (b) average ion flux as a function of frequency.

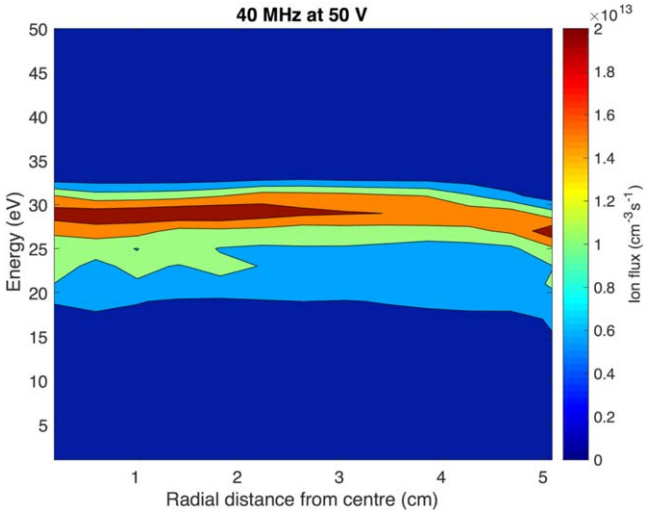

Figure 10. Geometry 1 total ion flux and energy as a function of electrode radius at 40 MHz and 50 V.

magnetic case. The shape is also different as the peak in the centre of the electrode no longer exists and only the edge effects appear to remain. This is a consequence of a complete change in the distribution of the plasma, as shown in figure 13. A proposed explanation for this is that the electrons cannot spread throughout the volume away from the areas of high density, as a result of being constrained to the magnetic field lines. The ions are still able to move, albeit through strong impedance, and move outwards away from the higher densities. This has been shown to be possible in field strengths of up to 2.3×10^4 G [37].

In high fields and low pressures the formation of filamentary structures within the plasma is reported [37–39]. These are not seen in these simulations as they have not been encountered at low field strengths (>0.9 T), but the cited works are significantly below the field strength within which the deposition removal process will be required to work. Moser *et al* have also shown a single filamentary structure in the B-field chamber which brought about a massive peak in etch rate at the location of the filament [17]. A further important factor to consider is the direction of the field. Although not analysed in this work the angle of the field to the mirror will also change the plasma dynamics. This is important for ITER as the field orientation will be different for each first mirror. Clearly a small vertical static B-field is able to cause significant changes in the plasma which are detrimental to etching. There are also indications that higher field strengths will induce filamentary structures which have been shown to cause localised etching. A detailed model is therefore needed to understand the effect of high magnetic fields in these low-temperature plasmas.

4. Conclusion

It has been shown that the geometry, set by the ITER design, will significantly influence the self bias of the created plasma and therefore the IEDF and etch behaviour. Furthermore, significant inhomogeneities across the electrode were observed, especially those induced by edge effects. These will cause any etching achieved to also be inhomogeneous resulting in potential surface profile changes to the mirrors. Voltage and frequency remain as variables which can tailor the IEDF to ideal values between 35 eV (threshold for Mo) and 25 eV (the estimated threshold for BeO), with the frequency being most significant due to narrower IEDFs at higher frequencies. However there is the consideration that metals, such as Mo, have been shown to have order of magnitude higher sputtering yields than oxides, such as BeO, when compared at higher energies [40]. With sputtering being a complicated process it is also known that threshold energies have an angular dependence which can cause sputtering below the threshold energy (usually measured with perpendicular ions) [41]. Therefore it is entirely possible that there is no energy at which the inhomogeneity of the IEDF can be ignored when using this method for deposition

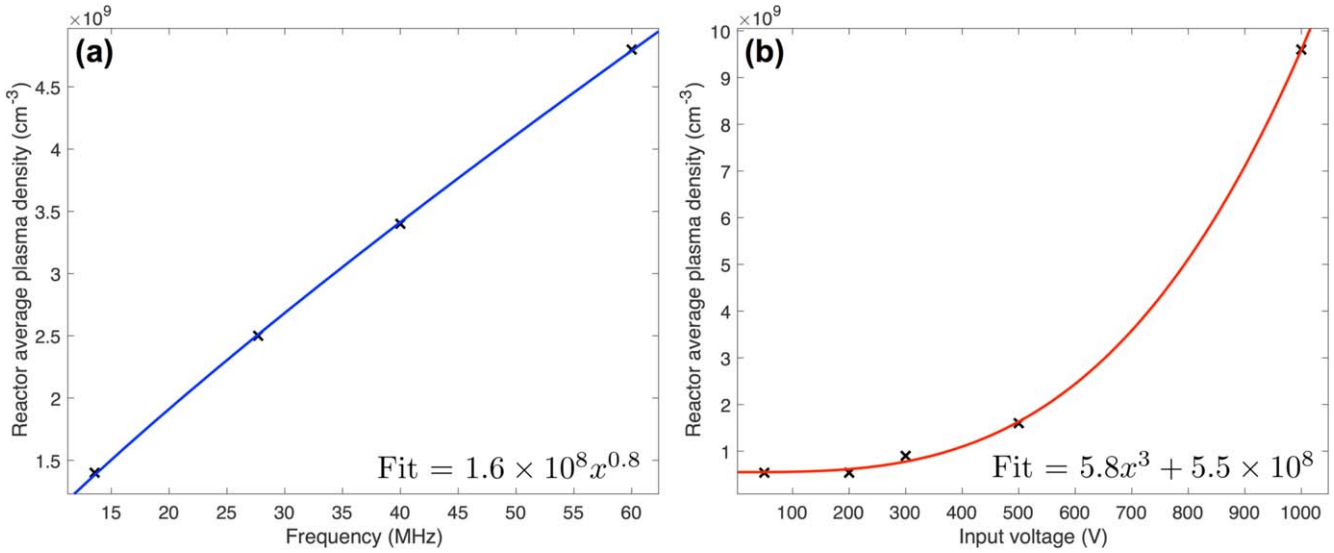

Figure 11. Plasma density as a function of (a) frequency and (b) voltage.

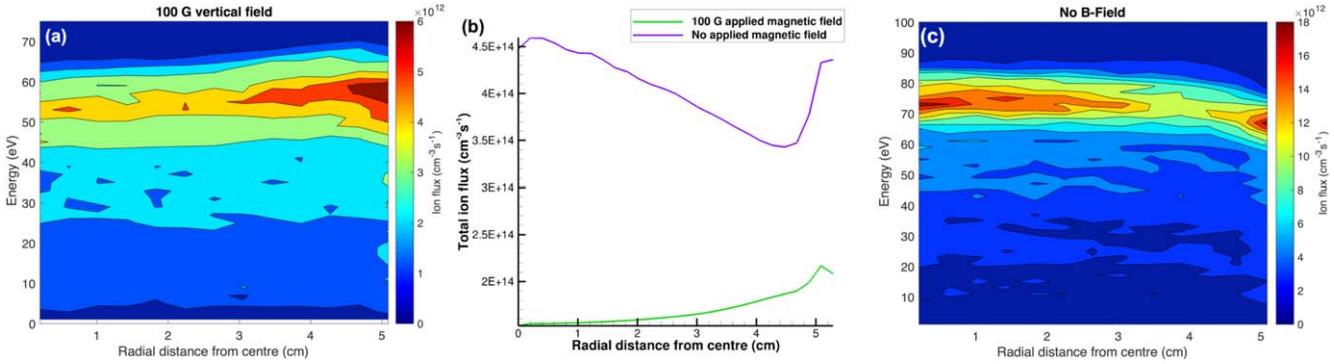

Figure 12. (a) Total ion flux and energy as a function of radial distance from the centre of the electrode in geometry 1 at 13.56 MHz, 130 V, 10 mTorr, and with a 100 G vertical magnetic field. (b) The total ion flux on the lower electrode with and without the magnetic field. (c) Total ion flux and energy as a function of radial distance for the same parameters but with no magnetic field.

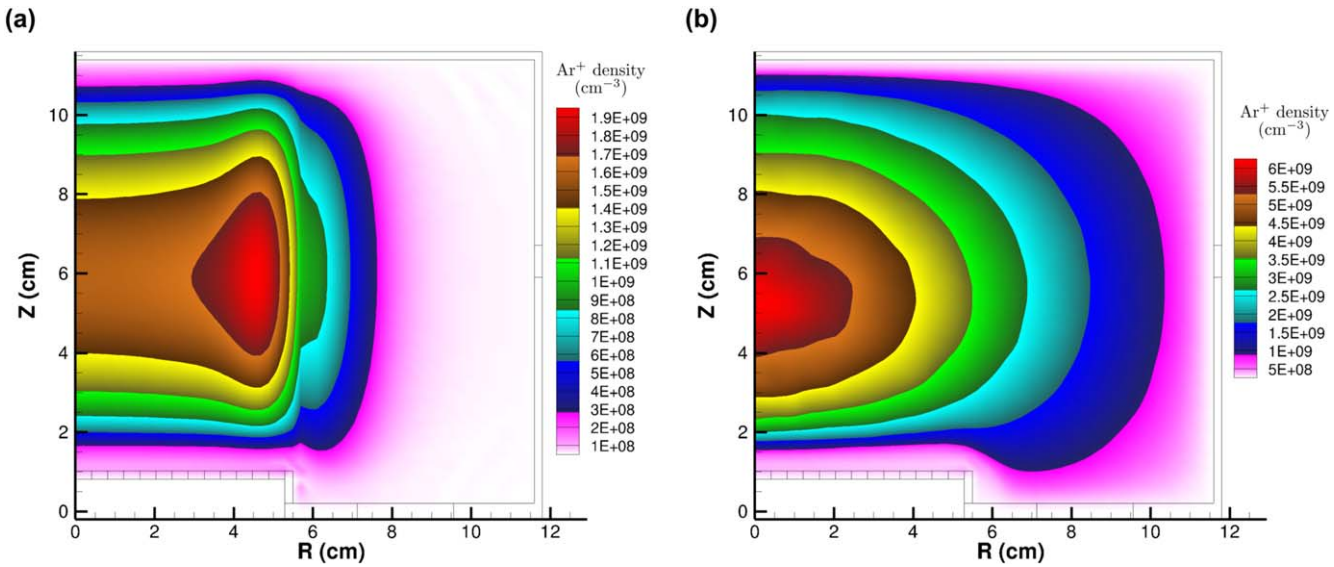

Figure 13. Ion densities in geometry 1 at 13.56 MHz, 130 V, at 10 mTorr. (a) Shows the densities with an applied 100 G vertical magnetic field and (b) shows the same simulation without the applied magnetic field.

removal if the mirror is to retain its shape and remain functional. It is also clear that the addition of magnetic fields cause significant changes to the plasma, even at relatively low magnitudes. Considering the complicated structure of ITER, and thus the many orientations that field lines may intersect with these mirrors, this area requires future investigation.

The recommendation is that further work is required for a full understanding of this method of deposition removal from fusion optics. It is clear that with the set geometries of ITER, and the impact that each geometry has on the plasma, there needs to be an assessment of each individual layout. In our opinion this is infeasible with an experimental campaign alone, owing to the large number of geometries, not only spatially varying but also within varying B field layouts and strengths. Through a combined effort of experiment and modelling an optimum set of parameters may be realised for individual cases.

Acknowledgments

Special thanks to Mark Kushner at the University of Michigan for all of his assistance in the set up and use of the HPEM model. This work was supported by the Engineering and Physical Sciences Research Council (EPSRC) [EP/L01663X/1 & EP/K018388/1].

Data access

All data created during this research are available by request from the University of York's York Research Database https://doi.org/10.15124/68cefa38-578d-4979-a5dd-24a4062172f6.

ORCID iDs

David Shaw https://orcid.org/0000-0001-5542-0334
Erik Wagenaars https://orcid.org/0000-0002-5493-3434

References

[1] Voitsenya V *et al* 2001 Diagnostic first mirrors for burning plasma experiments (invited) *Rev. Sci. Instrum.* **72** 475
[2] Donné A *et al* 2007 Chapter 7: diagnostics *Nucl. Fusion* **47** S337
[3] Rubel M, Coad J P, De Temmerman G, Hakola A, Hole D, Likonen J, Uytdenhouwen I and Widdowson A 2010 First mirrors test in JET for ITER: an overview of optical performance and surface morphology *Nucl. Instrum. Methods Phys. Res.* A **623** 818
[4] Ivanova D, Rubel M, Widdowson A, Petersson P, Likonen J, Marot L, Alves E, Garcia-Carrasco A and Pintsuk G 2014 An overview of the comprehensive first mirror test in JET with ITER-like wall *Phys. Scr.* **T159** 014011
[5] Ivanova D, Widdowson A, Likonen J, Marot L, Koivuranta S, Coad J P, Rubel M, Petersson P and De Temmerman G 2013 Assessment of cleaning methods for first mirrors tested in JET for ITER *J. Nucl. Mater.* **438** S1241
[6] Marot L, Linsmeier C, Eren B, Moser L, Steiner R and Meyer E 2013 Can aluminium or magnesium be a surrogate for beryllium: a critical investigation of their chemistry *Fusion Eng. Des.* **88** 1718
[7] Moser L, Marot L, Eren B, Steiner R, Mathys D, Leipold F, Reichle R and Meyer E 2015 Towards plasma cleaning of ITER first mirrors *Nucl. Fusion* **55** 063020
[8] Moser L, Steiner R, Leipold F, Reichle R, Marot L and Meyer E 2015 Plasma cleaning of ITER first mirrors in magnetic field *J. Nucl. Mater.* **463** 940
[9] Donnelly V M and Kornblit A 2013 Plasma etching: yesterday, today, and tomorrow *J. Vac. Sci. Technol.* A **31** 050825
[10] Hosokawa N, Matsuzaki R and Asamaki T 1974 RF sputter-etching by fluoro-chloro-hydrocarbon gases *Japan. J. Appl. Phys.* **13** 435
[11] Lieberman M A and Lichtenberg A J 2005 *Principles of Plasma Discharges and Materials Processing* (Hoboken, NJ: Wiley)
[12] Butler H S and Kino G S 1963 Plasma sheath formation by radio-frequency fields *Phys. Fluids* **6** 1346
[13] Moser L *et al* 2016 Plasma cleaning of beryllium coated mirrors *Phys. Scr.* **T167** 014069
[14] Moser L *et al* 2017 Investigation and plasma cleaning of first mirrors coated with relevant ITER contaminants: beryllium and tungsten *Nucl. Fusion* **57** 086019
[15] Leipold F *et al* 2016 Cleaning of first mirrors in ITER by means of radio frequency discharges *Rev. Sci. Instrum.* **87** 11D439
[16] Razdobarin A *et al* 2015 RF discharge for *in situ* mirror surface recovery in ITER *Nucl. Fusion* **55** 093022
[17] Moser L 2017 Plasma cleaning of diagnostic first mirrors for the nuclear fusion machine *PhD Thesis* University of Basel
[18] Bodhansky J, Roth J and Brossa F 1979 Formation of various coatings and their behaviour under particle bombardment *J. Nucl. Mater.* **85–86** 1145
[19] Yamamura Y and Tawara H 1996 Energy dependence of ion-induced sputtering yields from monatomic solids at normal incidence *At. Data Nucl. Data Tables* **62** 149
[20] Lee Y H, Zhou Z H, Danner D A, Fryer P M and Harper J M 1990 Chemical sputtering of Al_2O_3 by fluorine-containing plasmas excited by electron cyclotron resonance *J. Appl. Phys.* **68** 5329
[21] Day M E, Delfino M and Salimian S 1992 Low energy ion etching of aluminum oxide films and native aluminum oxide *J. Appl. Phys.* **72** 5467
[22] Kushner M J 2009 Hybrid modelling of low temperature plasmas for fundamental investigations and equipment design *J. Phys. D: Appl. Phys.* **42** 194013
[23] Kushner M J 2003 Modeling of magnetically enhanced capacitively coupled plasma sources: Ar discharges *J. Appl. Phys.* **94** 1436
[24] Lu J and Kushner M J 2001 Trench filling by ionized metal physical vapor deposition *J. Vac. Sci. Technol.* A **19** 2652
[25] Kinder R L and Kushner M J 2001 Wave propagation and power deposition in magnetically enhanced inductively coupled and helicon plasma sources *J. Vac. Sci. Technol.* A **19** 76
[26] Godyak V A and Piejak R B 1990 Abnormally low electron energy and heating-mode transition in a low-pressure argon rf discharge at 13.56 MHz *Phys. Rev. Lett.* **65** 996
[27] Kaganovich I D, Demidov V I, Adams S F and Raitses Y 2009 Non-local collisionless and collisional electron transport in low-temperature plasma *Plasma Phys. Control. Fusion* **51** 124003
[28] Weng Y and Kushner M J 1990 Method for including electron-electron collisions in Monte Carlo simulations of electron swarms in partially ionized gases *Phys. Rev.* A **42** 6192

[29] Song S-H and Kushner M J 2014 Role of the blocking capacitor in control of ion energy distributions in pulsed capacitively coupled plasmas sustained in $Ar/CF4/O_2$ *J. Vac. Sci. Technol.* A **32** 021306
[30] Huang S, Volynets V, Hamilton J R, Lee S, Song I-C, Lu S, Tennyson J and Kushner M J 2017 Insights to scaling remote plasma sources sustained in NF_3 mixtures *J. Vac. Sci. Technol.* A **35** 031302
[31] Huang S, Volynets V, Hamilton J R, Nam S K, Song I-C, Lu S, Tennyson J and Kushner M J 2018 Downstream etching of silicon nitride using continuous-wave and pulsed remote plasma sources sustained in $Ar/NF_3/O_2$ mixtures *J. Vac. Sci. Technol.* A **36** 021305
[32] Lu J and Kushner M J 2000 Effect of sputter heating in ionized metal physical vapor deposition reactors *J. Appl. Phys.* **87** 7198
[33] Eremin D 2015 Electromagnetic effects in capacitively coupled plasmas *Encyclopedia of Plasma Technology (EPLT)* ed J Leon Shohet (London: Taylor and Francis) pp 1–34
[34] Chabert P and Braithwaite N 2011 *Physics of Radio-Frequency Plasmas* (Cambridge: Cambridge University Press)
[35] Surendra M and Graves D B 1991 Capacitively coupled glow discharges at frequencies above 13.56 MHz *Appl. Phys. Lett.* **59** 2091
[36] Kinder R L and Kushner M J 2002 Wave propagation and power deposition in magnetically enhanced inductively coupled and helicon plasma sources *J. Vac. Sci. Technol.* A **19** 76
[37] Schwabe M, Konopka U, Bandyopadhyay P and Morfill G E 2011 Pattern formation in a complex plasma in high magnetic fields *Phys. Rev. Lett.* **106** 2
[38] Konopka U 2005 Complex plasmas in strong magnetic field environments *AIP Conf. Proc.* **799** 181–4
[39] Thomas E, Konopka U, Merlino R L and Rosenberg M 2016 Initial measurements of two- and three-dimensional ordering, waves, and plasma filamentation in the magnetized dusty plasma experiment *Phys. Plasmas* **23** 055701
[40] Kolasinski R D, Polk J E, Goebel D and Johnson L K 2007 Sputtering yield measurements at glancing incidence using a quartz crystal microbalance *J. Vac. Sci. Technol.* A **25** 236
[41] Eckstein W, Garciá-Rosales C, Roth J and László J 1993 Threshold energy for sputtering and its dependence on angle of incidence *Nucl. Instrum. Methods Phys. Res.* B **83** 95